Intrinsic high-temperature superconductivity in ternary iron selenides

Shin-Ming Huang,[1] Chung-Yu Mou,[1,2,3] and Ting-Kuo Lee[2]
[1]*Department of Physics, National Tsing Hua University, Hsinchu 30043, Taiwan*
[2]*Institute of Physics, Academia Sinica, Nankang, Taiwan*
[3]*Physics Division, National Center for Theoretical Sciences, P.O. Box 2-131, Hsinchu, Taiwan*
(Received 12 April 2013; published 15 November 2013)

We examine superconductivity in the mesoscopically mixed antiferromagnetic (AF) and superconducting (SC) phases of ternary iron selenides $K_yFe_{2-x}Se_2$. It is shown that the interlayer hopping and AF order are key factors to determine T_c of the SC phase. In general, the hopping will produce deformed Fermi surfaces (FSs) that tend to suppress superconductivity. However, contrary to the common expectation, we find that larger AF order actually results in larger SC order, which explains the observed relatively high T_c in these phases. Furthermore, our results indicate that by reducing the interlayer hopping appropriately, phase-separated $K_yFe_{2-x}Se_2$ may exhibit its intrinsic SC phase in the two-dimensional limit with a much higher T_c ($\sim$65 K) than what has been observed.

DOI: 10.1103/PhysRevB.88.174510 PACS number(s): 74.70.Xa, 74.20.Mn, 74.20.Rp

I. INTRODUCTION

The new discovery of ternary iron-selenide superconductors $A_yFe_{2-x}Se_2$ (A = K, Rb, Cs, and Tl)[1,2] opens an interesting route to explore the origin of high-temperature superconductivity in Fe-based superconductors. These materials have T_c up to 30 K, which is relatively high in comparison to the average T_c in the family of Fe-based superconductors. However, unlike many other Fe-based materials, in which the SC order gets suppressed in the presence of the antiferromagnetic (AF) order due to their strong competition, early resistivity measurements[1,3,4] surprisingly found that AF order and SC order coexisted while T_c was still kept relatively high. Further systematic investigations reveal that T_c's and the AF transition temperatures (T_N) of these materials exhibit similar trends: Both T_N and T_c are higher in the SC samples than those in the non-SC sample. This clearly implies that the coexisted antiferromagnetic ordering and superconductivity are not simply competing against each other.[5] In addition, it is found that the AF phase coincides with the $\sqrt{5}\times\sqrt{5}$ Fe-vacancy order with an extraordinarily large magnetic moment of $3.3\mu_B$/Fe.[6] These results prompt a critical examination and explanation on how the AF order with large moment can coexist with the SC order while T_c remains so high.

To explore the origin of relatively high T_c in ternary iron selenides, the nature of the phase with coexistence of SC and AF orders is further examined. A number of experiments[7–12] show that instead of being coexistent homogeneously, the SC and AF orders are phase separated at mesoscopic scales. In particular, the volume fraction of the SC phase is estimated to be less than 20% by using local probes.[9,11] Furthermore, it is shown that metallic behavior is exhibited in the SC phase,[9] while semiconducting behavior is found in the magnetic phase.[10] In addition, a heterostructure arrangement of SC and AF layers stacking alternatively is observed in transmission electron microscopy experiments,[7] consistent with the picture suggested by Charnukha *et al.*[10] A more direct visualization is obtained by recent scanning tunneling microscopy results,[13] in which two distinct regions along the *c* axis are clearly identified in the $K_xFe_{2-y}Se_2$ compound, SC KFe_2Se_2 (122 system), and insulating $K_xFe_{1.6}Se_2$ (245 system) with the $\sqrt{5}\times\sqrt{5}$ order. Furthermore, it is found that pure KFe_2Se_2 could exist in a metallic state without superconductivity but with weak charge density wave.[14]

On the theoretical side, much work has been devoted to understanding the homogeneous AF and SC phases of either the 122 or the 245 system.[15–24] Little is known about the mechanism of superconductivity in the combined system. Recently, Jiang *et al.*[25] investigated a bilayer heterostructure with both SC and AF phases. Based on the pair-hopping approximation between the SC and AF layers, it is shown that a drop of magnetic moment occurs in the AF layer when the temperature goes below the SC transition, in agreement with the observation of neutron scattering experiments.[6] Since the effect on SC phase due to the AF order is found to be quite substantial,[13,14] it is interesting to examine what is the effect of AF order on superconductivity, especially in the presence of such strong AF order in the iron-vacancy-ordering phase.

In this work, we investigate superconductivity in a bilayer system with an iron-vacancy-free layer on top of an iron-vacancy-ordered AF layer (245). The iron-vacancy-free layer is nominally taken to be the 122 system with fitted band structures. The electronic structures are examined under different strengths of interlayer hopping, interlayer spin coupling, and AF order. It is shown that both the interlayer hopping and interlayer spin coupling generally suppress superconductivity. In particular, the interlayer hopping would result in deformed Fermi surface structures that tend to frustrate the coupling of SC orders on Fermi surfaces. However, unexpectedly we find that for fixed hopping amplitude, larger AF orders actually result in larger SC orders, which explains the observed relatively high T_c and trends of T_c versus the AF transition temperature T_N (Ref. 5) in these phases. Our results imply that in the two-dimensional (2D) limit, the pure SC phase in phase-separated ternary iron selenides may have a much higher T_c, being around 65 K.

II. THEORETICAL MODEL

We start by modeling the phase-separated region of $K_yFe_{2-x}Se_2$ as a bilayer junction,[25] shown in Fig. 1. Here the top layer is nominally taken as the SC 122 phase and the bottom layer is the AF 245 phase. The system is governed by

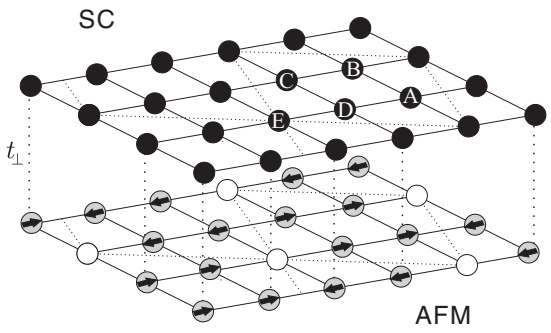

FIG. 1. Coupled 122-245 bilayer junction. The top lattice is the SC 122 layer and the bottom one is the AF 245 layer. The dotted lines enclose the unit cell in each layer, and its basis contains five Fe atoms, denoted by A, B, C, D, and E. The E sites in the 245 layer are vacancy positions, denoted by empty circles.

the Hamiltonian

$$H = H_{122} + H_{245} + H_\perp^t + H_\perp^J. \tag{1}$$

Here H_{122} and H_{245} are the individual Hamiltonians for the 122 and 245 layers, $H_\perp^t$ is the Hamiltonian for interlayer hopping, and $H_\perp^J$ is the Hamiltonian for the interlayer spin coupling. To include multiorbital effect, we shall focus on the most relevant orbitals by considering two orbitals only, $d_{\overline{x}z}$ and $d_{\overline{y}z}$, with $\overline{x}$ or $\overline{y}$ being along the nearest neighbor Fe-Fe direction. In the following, c_τ (d_τ) denotes the electron annihilation operator for the 122 (245) layer with $\tau = 1$ and 2 representing $d_{\overline{x}z}$ and $d_{\overline{y}z}$, respectively. All the energies are in unit of electron volts (eV).

For the 122 layer, H_{122} contains a hopping term and a pairing term. The hopping term is described by Das and Balatsky,[15] which yields Fermi surface (FS) pockets at $(\pi,0)$ and $(0,\pi)$ in the 1Fe/cell picture. The pairing term with an attractive potential within nearest-neighbor and next-nearest-neighbor sites is given by

$$H_\Delta = -V_1 \sum_{i,\bar{d}=\bar{x},\bar{y}} \sum_{\tau,\sigma} c^\dagger_{\tau;i+\bar{d},\sigma} c^\dagger_{\tau;i,-\sigma} c_{\tau;i,-\sigma} c_{\tau;i+\bar{d},\sigma} - V_2 \sum_{i,\bar{d}=\bar{x}\pm\bar{y}} \sum_{\tau,\sigma} c^\dagger_{\tau;i+\bar{d},\sigma} c^\dagger_{\tau;i,-\sigma} c_{\tau;i,-\sigma} c_{\tau;i+\bar{d},\sigma}. \tag{2}$$

Here σ is the spin index and V_1 and V_2 are positive.

To describe the 245 layer, we note that the unit cell with one vacancy contains eight orbitals of electrons. The tight-binding model that respects the $I/4m$ symmetry of $\sqrt{5}\times\sqrt{5}$ Fe-vacancy order is constructed in Ref. 23. Following Ref. 23, H_{245} is constructed by removing $d_{\overline{x}\overline{y}}$ with parameters being modified. The parameters for hoppings are $t_{11,\bar{x}} = -t_{11,\bar{y}} = 0.3$, $t'_{11,\bar{x}} = 0.2$, $t'_{11,\bar{y}} = 0.15$, $t_{11,\bar{x}+\bar{y}} = -0.15$, $t_{11,\bar{x}-\bar{y}} = t'_{11,\bar{x}+\bar{y}} = -t'_{11,\bar{x}-\bar{y}} = -0.08$, $t_{12,\bar{x}} = t_{12,\bar{y}} = t'_{12,\bar{x}} = 0$, $t_{12,\bar{x}+\bar{y}} = t'_{12,\bar{x}+\bar{y}} = t'_{12,\bar{x}-\bar{y}} = -0.02$, and $\Delta = 0.08$. Here $t_{\tau\tau',\overline{R}}$ ($t'_{\tau\tau',\overline{R}}$) are for intracell (intercell) hoppings between orbitals τ and τ' along $\overline{R}$ directions and Δ is the site energy difference between $d_{\overline{x}z}$ and $d_{\overline{y}z}$ orbitals. Other hopping parameters can be obtained from above by using symmetries of the system, for example, $t_{22,\bar{x}} = t_{11,\bar{y}}$ as a result of the fourfold rotational symmetry. In addition to hopping, the interaction between electrons in the 245 layer is given by the generalized Hubbard model,[23]

$$H_I = \sum_i \sum_{I=A,B,C,D} \Bigg\{ U \sum_\tau n^{(d)}_{\tau I,i\uparrow} n^{(d)}_{\tau I,i\downarrow} + \Bigg[\left(U' - \frac{J_H}{2} \right) n^{(d)}_{1I,i} n^{(d)}_{2I,i} - 2J_H \mathbf{S}^{(d)}_{1I,i} \cdot \mathbf{S}^{(d)}_{2I,i} + J_C (d^\dagger_{1I,i\uparrow} d^\dagger_{1I,i\downarrow} d_{2I,i\downarrow} d_{2I,i\uparrow} + \text{H.c.}) \Bigg] \Bigg\}. \tag{3}$$

Here A, B, C, and D denote Fe atoms in the unit cell, as illustrated in Fig. 1. The on-site interaction parameters follow the relations $U' = U - 2J_H$, $J_C = J_H$, and $J_H = 0.2U$. The chemical potential is used to control the particle density per iron at $n = 2$.

As two layers couple, the unit cell of the 122 layer is enlarged as that of the 245 layer. We shall denote Fe atoms by A, B, C, D. Here E is the position of the vacancy in 245, as illustrated in Fig. 1. $H_\perp^t$ is given by

$$H_\perp^t = t_\perp \sum_i \sum_{I=A,B,C,D} \sum_{\tau,\sigma} (c^\dagger_{\tau I;i\sigma} d_{\tau I;i\sigma} + d^\dagger_{\tau I;i\sigma} c_{\tau I;i\sigma}). \tag{4}$$

On the other hand, the interlayer spin interaction $H_\perp^J$ is given by

$$H_\perp^J = J_\perp \sum_i \sum_{I=A,B,C,D} \sum_{\tau,\tau'} \mathbf{S}^{(c)}_{\tau I,i} \cdot \mathbf{S}^{(d)}_{\tau' I,i}. \tag{5}$$

Here $\mathbf{S}^{(c)}_{\tau I,i}$ is the spin operator of electrons in the 122 layer, while $\mathbf{S}^{(d)}_{\tau' I,i}$ is that of electrons in the 245 layer. For Fe-based superconductors, $J_\perp$ is found to be in the range of 1–5 meV.[26] We shall set $J_\perp$ to be a nominal value of 10 meV in this work.

In the following, we shall first turn off $J_\perp$ and consider effects of $t_\perp$. The distance between two nearest vacancies will be set as unity and their directions are denoted as x and y. For the isolated 245 layer, the mean-field solutions of the AF order are shown in Fig. 2. Since we shall focus on the effects of AF order on superconductivity, AF orders are treated as boundary conditions and will not be solved self-consistently later when interlayer couplings are turned on. Hence these values obtained in Fig. 2 will be adopted later even when the interlayer couplings are turned on. It is seen that the antiferromagnetism is weak when $U \lessapprox 1.5$ and is strong with saturated magnetization when $U > 1.5$. In Fig. 3, we show the energy dispersions of the AF states with $U = 0$, 1.0, 1.5, and 2.0, at which the development of the antiferromagnetism is at the beginning, in the middle, right before the jump, and at the saturation, respectively. Clearly, H_{245} reproduces the quasinested FS and the expected block checkerboard antiferromagnetism [with $\mathbf{q} = (\pi,\pi) \equiv \mathbf{Q}$] as the Hubbard U increases above the critical value, $U \approx 0.5$. The minimal gap is along the diagonal ($\Gamma - M$) direction and is smaller than 0.05 eV before the saturation. When $U > 1.5$, a large AF gap, $2\Delta_{\text{AF}}$, opens. However, for $1.0 < U < 1.5$, we find that although bands are expelled to higher energy as U increases, the energy gap near the chemical potential decreases, resulting in the AF gap at $U = 1.0$ ($\Delta_{\text{AF}} = 0.046$) being larger than that at $U = 1.5$ ($\Delta_{\text{AF}} = 0.023$). Note that with two d orbitals, one cannot produce as detailed characteristics of the band structure

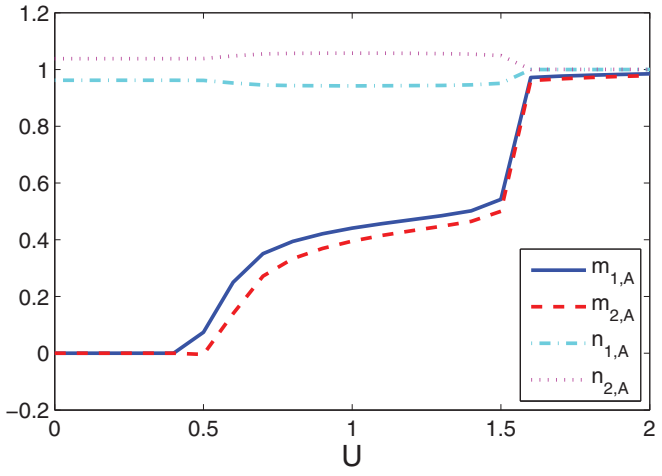

FIG. 2. (Color online) Mean-field solutions of the checkerboard AF states of H_2 for the Hubbard U being up to two. Magnetic moments ($m = n_\uparrow - n_\downarrow$) and particle densities ($n = n_\uparrow + n_\downarrow$) at sites A and B for orbitals 1 and 2 are respectively displayed. The antiferromagnetism arises at the critical point $U = 0.5$, and it jumps to being fully magnetized at $U = 1.6$.

as those obtained by the first-principles calculations.[16,23] However, important relevant features are reproduced with the AF state being a gapped insulator and the AF order being in agreement with the experimental observation.

After the interlayer hopping is included, FSs of the 122 layer start to deform as shown in Fig. 4. Here three values of $t_\perp$ ($t_\perp = 0.05$, 0.1, and 0.15) for $U = 0.5$, 1.0, 1.5, and 2.0 are shown. Panels in the first row are for $t_\perp = 0.05$, the second row are for $t_\perp = 0.1$, and the third one are for $t_\perp = 0.15$. On the other hand, columns from the left to the right are cases with $U = 0.5$, $U = 1.0$, $U = 1.5$, and $U = 2.0$, respectively. It is seen that for large U with large AF orders, FS sheets at $(\pi,0)$ are always disconnected from those at $(0,\pi)$; while for weak AF orders, interlayer hopping deforms FS pockets

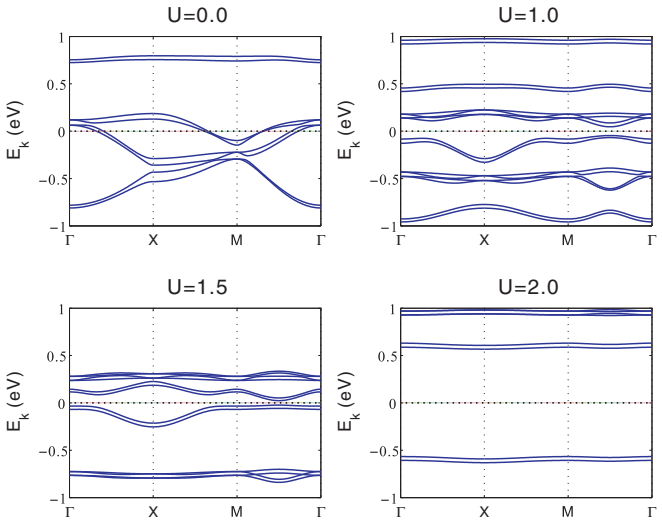

FIG. 3. (Color online) Energy dispersions in the range $(-1,1)$ of the AF states for H_{245} at $U = 0$, 1.0, 1.5, and 2.0, respectively. It is clear that above $U \approx 1.5$, a large AF gap, $\Delta_{\rm AF}$, opens.

at $(\pi,0)$ and $(0,\pi)$ so that they start to connect with each other and, consequently, more FS pockets emerge and the electronic structure becomes very complicated. In particular, as $t_\perp$ increases or U decreases, apparent FS pockets emerge around Γ and M, which are mainly contributions from the AF state.

III. RESULTS

We first characterize SC states in the 122 system. For this purpose, we note that since A_g (s wave) and B_g (d wave) are the two major competing order parameters,[24] we shall only consider these pairing symmetries. In addition, in constructing SC order parameters, one needs to impose point-group symmetries. Therefore, the $d_{\overline{yz}}$-orbital pairs are obtained from the $d_{\overline{xz}}$-orbital pairs, e.g., $\langle c_{2A;i} c_{2B;i}\rangle = \pm\langle c_{1B;i} c_{1C;i}\rangle$, where $\pm$ denotes s wave/d wave. In addition, due to the presence of vacancies, translation symmetry will not always hold, e.g., $|\langle c_{1D;i} c_{1E;i}\rangle| \neq |\langle c_{1A;i} c_{1D;i}\rangle|$.

Given the pairing symmetry, T_c is obtained by solving the Bethe-Salpeter equation

$$\Delta^{ij}(K) = -\lambda \sum_{K'} \Delta^{m'n'}(K) G_{mm'}(K') G_{nn'}(-K') V^{ij}_{mn}(K,K'). \tag{6}$$

Here $K = (\mathbf{k}, i\omega_n)$ with $\omega_n = (2n+1)\pi kT$ being the Matsubara frequency, the indices i and j are orbital-sublattice indices containing both orbital and site labels, and implicit summation over orbital indices m, n, m', and n' is taken. Δ is the pairing amplitude, λ is the eigenvalue, and V is the pairing interaction. $G_{mm'}$ is the Green's function with orbital indices m,m' defined by

$$G_{mm'}(\mathbf{k}, i\omega_n) = \sum_\mu \frac{A_{m\mu}(\mathbf{k}) A^*_{m'\mu}(\mathbf{k})}{i\omega_n - \xi_\mu(\mathbf{k})}. \tag{7}$$

Here ξ_μ is the energy of the band μ. $A_{m\mu}$ is the transformation matrix that connects the orbital basis $\psi_m(\mathbf{k})$ to the eigenenergy basis $\gamma_\mu(\mathbf{k})$ via the relation $\psi_m(\mathbf{k}) = \sum_\mu A_{m\mu}(\mathbf{k})\gamma_\mu(\mathbf{k})$. It is more convenient to work in the k space by transforming Eq. (6) into band representation using the transformation matrix $A_{m\mu}$. We shall assume that pairing is among the intraband and decompose the interaction into different bases $g_a(\mathbf{k})$,

$$V^{ij}_{mn}(\mathbf{k},\mathbf{k}') = -\delta_{im}\delta_{jn} \sum_a \mathcal{V}^{ij}_a g_a(\mathbf{k}) g^*_a(\mathbf{k}'). \tag{8}$$

By multiplying both sides of Eq. (6) by $A_{i\mu}(-\mathbf{k})A_{j\mu}(\mathbf{k})$ and summing over i, j, and then performing the Matsubara frequency summation, Eq. (6) is transformed into the representation in the band basis

$$\Delta_\mu(\mathbf{k}) = 2 \sum_{a'} \sum_{i' \leqslant j'} \Re[g_{a'}(\mathbf{k}) A_{i'\mu}(-\mathbf{k}) A_{j'\mu}(\mathbf{k})] \mathcal{J}^{i'j'}_{a'}, \tag{9}$$

with $\mathcal{J}^{ij}_a$ being the order parameter satisfying a self-consistent equation

$$\mathcal{J}^{ij}_a = \lambda \sum_{a'} \sum_{i' \leqslant j'} \mathcal{V}^{ij}_a \mathcal{K}^{ij,i'j'}_{a,a'} \mathcal{J}^{i'j'}_{a'}. \tag{10}$$

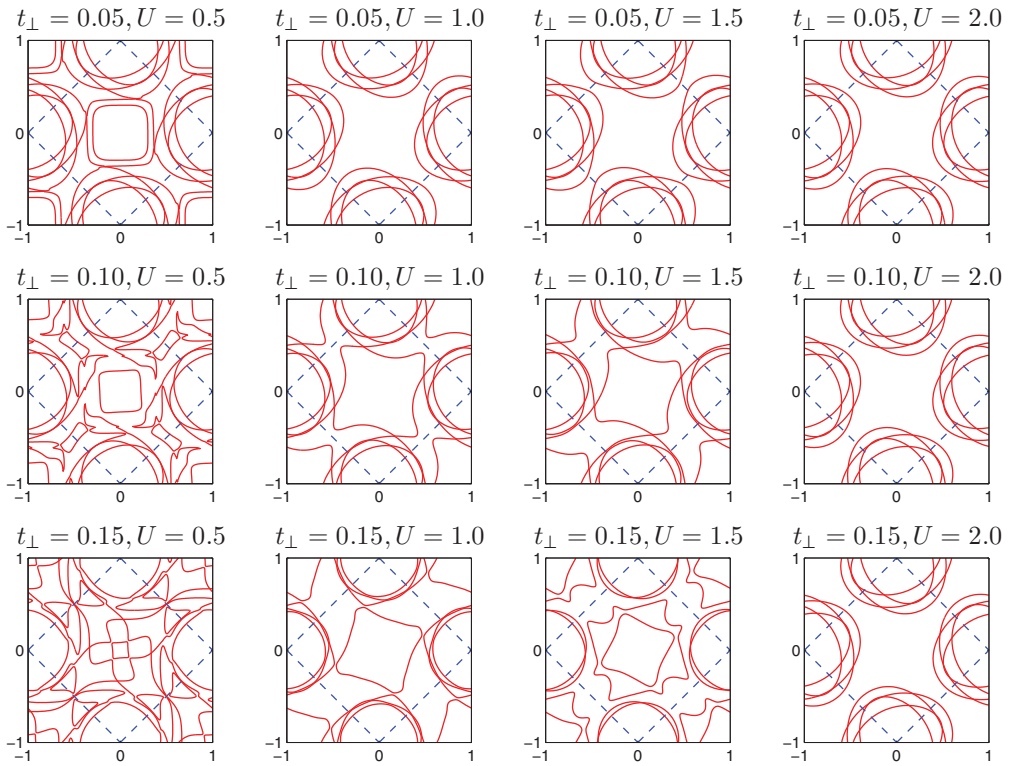

FIG. 4. (Color online) The FS contours in the absence of superconductivity when the two layers 122-245 couple together. The panels in the first row are for $t_\perp = 0.05$; those in the middle are for $t_\perp = 0.1$; and those in the last row are for $t_\perp = 0.15$. The panels in the first column are for $U = 0.5$, the second for $U = 1.0$, the third for $U = 1.5$, and the fourth for $U = 2.0$. The unit of the x axis is k_x/π and that of the y axis is k_y/π. Here dashed lines are the magnetic Brillouin zone boundaries and the AF order parameters are those obtained from the isolated 245 layer.

Here $\Delta_\mu(\mathbf{k}) \equiv \sum_{m,n} A_{m\mu}(-\mathbf{k})A_{n\mu}(\mathbf{k})\Delta^{mn}(\mathbf{k})$ and $\mathcal{K}^{ij,i'j'}_{aa'}$ is given by

$$\mathcal{K}^{ij,i'j'}_{aa'} = \frac{2}{N}\sum_\mu \sum_{\mathbf{k}} \Re[g_a(\mathbf{k})A_{i\mu}(-\mathbf{k})A_{j\mu}(\mathbf{k})] \times \Re[g_{a'}(\mathbf{k})A_{i'\mu}(-\mathbf{k})A_{j'\mu}(\mathbf{k})]\chi_\mu(\mathbf{k}) \quad (11)$$

with $\chi_\mu(\mathbf{k}) \equiv \tanh[\xi_\mu(\mathbf{k})/2kT]/2\xi_\mu(\mathbf{k})$. The SC state is found by solving eigenvalues and eigenvectors of the vertex $\hat{\mathcal{V}}\hat{\mathcal{K}}$ in Eq. (10) with T_c being obtained when $\lambda = \mathbf{1}$.

In Fig. 5, we examine the SC gap functions near the FSs defined by

$$\Delta(\mathbf{k}) = \sum_\mu \Delta_\mu(\mathbf{k})\Theta(\epsilon - |\xi_\mu(\mathbf{k})|). \quad (12)$$

Here ϵ is a small energy cutoff that restricts the gap function to be exhibited near the FS. Three different $t_\perp$, 0.05, 0.10, and 0.15 at $U = 1.5$ are shown for the$s$ wave in the left column and the d wave in the right column. Clearly, one sees that as the interlayer hopping increases and the FS contours start to deform, the gap functions become more anisotropic and the condensation energy decreases. However, the characters of both the s wave and the d wave are clearly kept on the deformed FS as shown in Fig. 5 for $t_\perp = 0.15$, where zeros of $\Delta(\mathbf{k})$ are present for the d wave on the central FS, but they do not exist for the s wave. This symmetry property makes the d wave more disadvantageous than the s wave when two layers are strongly coupled. Hence the d wave is more sensitive to the interlay coupling than the s wave. Note that since there is only an indirect correlation between particles with momentum $\mathbf{k}$ and $\mathbf{k} + \mathbf{Q}$ via the 245 layer, $\Delta(\mathbf{k})$ does not have to be equal to $\Delta(\mathbf{k} + \mathbf{Q})$.

We now examine the effects of the interlayer hopping and the AF order on the SC transition. First, we note that similar to the situations in iron pnictides,[27] V_1 tends to favor the d wave, while V_2 favors the s wave, and the phase boundary is at $V_1/V_2 \sim 0.78$. To be concrete, we shall set $V_1 = 0.175$ and $V_2 = 0.25$ and focus on T_c of the s wave. Similar behavior is found for the d wave. Figure 6(a) shows T_c of the s-wave SC order versus $t_\perp$ for different values of U. Clearly, for a given AF order (fixed by U), it is seen that T_c always gets suppressed by $t_\perp$. However, for fixed $t_\perp$, when U increases, the change of T_c is nonmonotonic (due to nonmonotonic Δ_{AF}) and T_c is only weakly suppressed at $U \sim 2$. Further analysis shown in Fig. 6(b) indicates that the penetrated AF order into the 122 layer has the inverse trend as that of T_c. These behaviors can be understood by examining FS structures. A comparison of Figs. 4 and 6(a) shows that the suppression of the SC order is due to the deformed FS structures induced by the interlayer hopping. The deformed FS structures generally frustrate the coupling of SC orders on FSs and thus suppress the SC order. However, in the presence of strong AF order, the 245 layer is insulating with a gap. Since the coherence length ξ_{AF} of an AF phase is $\xi_{\mathrm{AF}} \sim \frac{\hbar v_F}{\Delta_{\mathrm{AF}}}$ with v_F being the characteristic

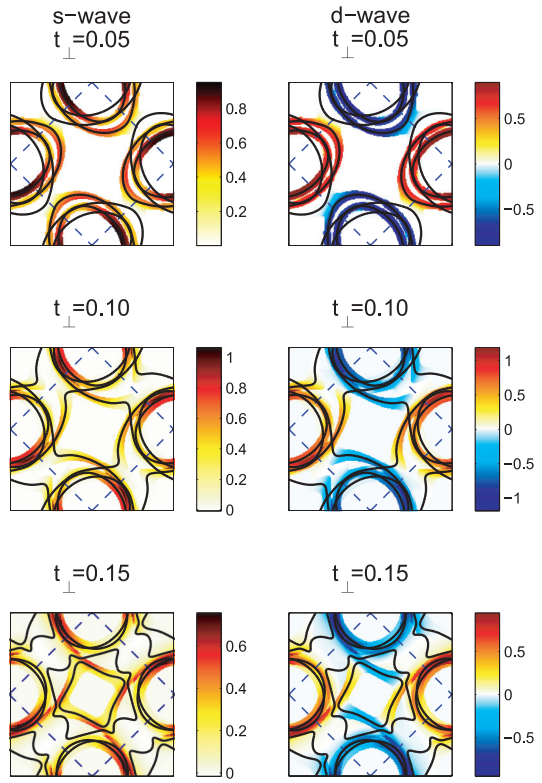

FIG. 5. (Color online) Gap functions $\Delta(\mathbf{k})$ of the s wave (left column) and of the d wave (right column) near FSs at T_c. Three cases of $t_\perp$'s are compared: $t_\perp = 0.05$, $t_\perp = 0.10$, and $t_\perp = 0.15$. Other common parameters are $V_1 = 0.175$, $V_2 = 0.225$, and $U = 1.5$. The scale is arbitrary.

Fermi velocity, a large AF gap implies a short penetration depth of the AF order into the SC layer. Hence the induced deformation of FS structure is weak, which leads to weak suppression of superconductivity. Note that since the interlayer hopping between the AF layer and the SC layer suppresses T_c, these results imply that the pure SC phase has a higher T_c. If one takes $t_\perp = 0.15$ and $U = 2$ as a reasonable estimation of phase-separated ternary iron selenides, the real SC transition

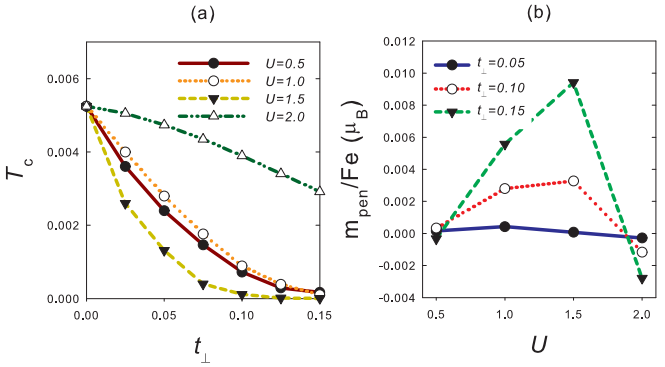

FIG. 6. (Color online) (a) Suppression of T_c versus $t_\perp$ of the s wave for different U's. Here $V_1 = 0.175$ and $V_2 = 0.25$. Note that T_c of the d wave has a similar trend but the suppression is more severe. (b) Average moment that penetrates into the 122 layer in the normal state for different U and $t_\perp$.

is around 65 K, which is comparable to the highest observed T_c in the family of iron selenides.[14] The suppression of T_c due to the interlayer hopping $t_\perp$ is also studied by Berg *et al.*[28] for a one-band negative U model, in which it is shown that the leading order correction to the pairing susceptibility is negative and is proportional to $t_\perp^2$. As a result, in their model, T_c is suppressed by the order of $t_\perp^2$ for small $t_\perp$. The susceptibility suppression also happens in our case as one can see that in Eq. (11),$t_\perp$ will change ξ_μ and $A_{i\mu}$ and thus values of $\mathcal{K}$. However, due to the multiorbital nature of our model, the behavior of T_c at small $t_\perp$ does not follow simple quadratic behavior. Only for weak suppression of T_c at large U shown in 6(a), we find that suppression of T_c is quadratic in $t_\perp$, in agreement with results found in Ref. 28.

Finally we examine the effects of interlayer spin interaction $H_\perp^J$ on superconductivity. For this purpose, we first note that $H_\perp^J$ only characterizes single particle scattering in the 122 layer and the 245 layer, respectively. Hence the effective Hamiltonian for scatterings of Cooper pairs in the 122 layer must be second order in $H_\perp^J$. To the second order in the perturbation theory, scattering of two particles for the particle-particle channel in the 122 layer is given by $T_\perp^{(2)} \equiv H_\perp^J (E_0 - H_0)^{-1} H_\perp^J$, where E_0 is the unperturbed ground state energy, $H_0 = H_{122} + H_{245}$, and $H_0 - E_0$ is the energy excitation for the intermediate state. During the scattering of two particles in the 122 layer, scatterings in the 245 layer are captured by the magnetic susceptibility with the major weight being in particle-hole excitations. Since the particle-hole excitation energy of an AF insulator is the sum of the energies for two quasiparticles above the AF gap, the change of energy for the intermediate state during scattering of Cooper pairs is at least $2\Delta_{\mathrm{AF}}$. By neglecting the dispersion of energy spectrum, we find $(E_0 - H_0)^{-1} \approx -(2\Delta_{\mathrm{AF}})^{-1}$. Therefore, after taking an average over d electrons of the 245 layer, the effective intraorbital pairing Hamiltonian due to interlayer spin interaction is given by

$$\delta H_\Delta = V_J \sum_{i,\bar{d}=\bar{x},\bar{y},\bar{x}\pm\bar{y}}{}' \sum_{\tau,\sigma} c^\dagger_{\tau;i+\bar{d},\sigma} c^\dagger_{\tau;i,-\sigma} c_{\tau;i,-\sigma} c_{\tau;i+\bar{d},\sigma}, \quad (13)$$

where the summation does not include E sites and $V_J = \frac{3J_\perp^2}{4\Delta_{\mathrm{AF}}}$. We note that it is a repulsive interaction for Cooper pairs and hence the interlayer interaction tends to suppress superconductivity. In Fig. 7, we examine changes of T_c for $J_\perp = 0.01$ in three different U's with corresponding V_J being 0.0016, 0.0032, and 0.0001. It is seen that similar to the effects of $t_\perp$, T_c gets suppressed but the suppression is nonmonotonic and the variation of suppression is less than the suppression due to different U's. In particular, similar to the suppression by $t_\perp$, a stronger AF phase gets less suppression in superconductivity. The mechanism behind the behavior of suppression of T_c is clearly due to the dependence of effective pairing strength V_J being inversely proportional to Δ_{AF}. In addition to direct interlayer spin coupling, in real materials, $J_\perp$ may arise from superexchange interaction between the 122 and 245 layers. In that situation, $J_\perp$ is proportional to $\frac{t_\perp^2}{U}$. Since $U \sim \Delta_{\mathrm{AF}}$, we have $J_\perp \sim \frac{t_\perp^2}{\Delta_{\mathrm{AF}}}$. As a result, not only the wave-function hybridization due to $t_\perp$ but also the interlayer spin interaction resulted from $t_\perp$ suppressing pairing and resulted in nonmonotonic suppression

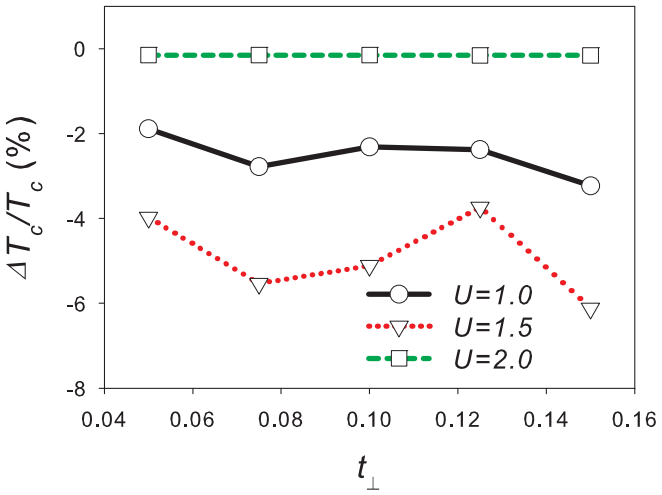

FIG. 7. (Color online) Suppression of s-wave T_c ($\Delta T_c/T_c$) versus $t_\perp$ for a given interlayer spin interaction $J_\perp$ under three different U's in the 245 system. Here $V_1 = 0.175$ and $V_2 = 0.25$ are same as those adopted in Fig. 6. The interlayer spin coupling $J_\perp$ is 0.01 with the corresponding V_J's for the $U = 1.0$, 1.5, and 2.0 cases being 0.0016, 0.0032, and 0.0001, respectively.

of T_c with T_c being less suppressed for large Δ_{AF}. Hence while both interlayer hopping and interlayer spin couplings suppress superconductivity, a large AF order in the 245 layer can result in stronger superconductivity in the 122 layer.

IV. SUMMARY

In summary, we have found that the existence of a large magnetic moment in the AF phase is the key reason for why the phase-separated ternary iron selenides can maintain a relatively high T_c despite the strong competition between SC and AF orders. Based on a minimal bilayer model with both the 122 and 245 phases, we show that proximity effects of the AF order on the SC order generally result in the deformation of FS due to the interlayer hopping and Cooper pair scatterings due to the interlayer spin interaction. It is shown that the deformed FSs generally frustrate coupling of SC orders and result in the suppression of superconductivity. In addition, the interlayer spin coupling generates repulsive Cooper pair scattering and it also tends to suppress superconductivity. However, when the AF phase has a large AF order, it is insulating with a large gap and the penetration of the AF order into the SC layer is suppressed. As a result, the superconductivity is protected against interlayer hopping and interlayer spin coupling when Δ_{AF} is much larger than the interlayer hopping.

While our results are consistent with experimental observations made so far, there are a number of experimental observations of 3D-like FSs in the phase-separated region.[16,17,29] To account for these experimental results, it would require a relatively large interlayer coupling. Since the interlayer hopping between the AF and SC layers suppresses T_c, our results imply that a 2D-like system may be more preferable for higher T_c. In fact, the real SC phase in phase-separated ternary iron selenides may have a higher T_c up to 65 K, which is comparable to the highest observed T_c in the family of iron selenides.[30]

ACKNOWLEDGMENTS

We thank Professor Ming-Che Chang for useful discussions. This work was supported by the National Science Council of Taiwan.

[1] J. Guo, S. Jin, G. Wang, S. Wang, K. Zhu, T. Zhou, M. He, and X. Chen, Phys. Rev. B **82**, 180520(R) (2010).
[2] A. F. Wang, J. J. Ying, Y. J. Yan, R. H. Liu, X. G. Luo, Z. Y. Li, X. F. Wang, M. Zhang, G. J. Ye, P. Cheng, Z. J. Xiang, and X. H. Chen, Phys. Rev. B **83**, 060512(R) (2011).
[3] M. H. Fang, H. D. Wang, C. H. Dong, Z. J. Li, C. M. Feng, J. Chen, and H. Q. Yuan, Europhys. Lett. **94**, 27009 (2011).
[4] D. M. Wang, J. B. He, T.-L. Xia, and G. F. Chen, Phys. Rev. B **83**, 132502 (2011).
[5] R. H. Liu, Europhys. Lett. **94**, 27008 (2011).
[6] W. Bao, Q. Huang, G. F. Chen, M. A. Green, D. M. Wang, J. B. He, X. Q. Wang, and Y. Qiu, Chin. Phys. Lett. **28**, 086104 (2011).
[7] Z. Wang, Y. J. Song, H. L. Shi, Z. W. Wang, Z. Chen, H. F. Tian, G. F. Chen, J. G. Guo, H. X. Yang, and J. Q. Li, Phys. Rev. B **83**, 140505(R) (2011).
[8] F. Chen, M. Xu, Q. Q. Ge, Y. Zhang, Z. R. Ye, L. X. Yang, J. Jiang, B. P. Xie, R. C. Che, M. Zhang, A. F. Wang, X. H. Chen, D. W. Shen, J. P. Hu, and D. L. Feng, Phys. Rev. X **1**, 021020 (2011).
[9] Y. Texier, J. Deisenhofer, V. Tsurkan, A. Loidl, D. S. Inosov, G. Friemel, and J. Bobroff, Phys. Rev. Lett. **108**, 237002 (2012).
[10] A. Charnukha, A. Cvitkovic, T. Prokscha, D. Pröpper, N. Ocelic, A. Suter, Z. Salman, E. Morenzoni, J. Deisenhofer, V. Tsurkan, A. Loidl, B. Keimer, and A. V. Boris, Phys. Rev. Lett. **109**, 017003 (2012).
[11] Z. Shermadini, H. Luetkens, R. Khasanov, A. Krzton-Maziopa, K. Conder, E. Pomjakushina, H.-H. Klauss, and A. Amato, Phys. Rev. B **85**, 100501(R) (2012).
[12] Z. M. Stadnika, P. Wanga, J. Żukrowskib, H. D. Wang, C. H. Dong, and M. H. Feng, J. Alloys Compd. **549**, 288 (2013).
[13] W. Li, H. Ding, P. Deng, K. Chang, C. Song, K. He, L. Wang, X. Ma, J. P. Hu, X. Chen, and Q. K. Xue, Nat. Phys. **8**, 126 (2012).
[14] W. Li, H. Ding, Z. Li, P. Deng, K. Chang, K. He, S. Ji, L. Wang, X. Ma, J. P. Hu, X. Chen, and Q. K. Xue, Phys. Rev. Lett. **109**, 057003 (2012).
[15] T. Das and A. V. Balatsky, Phys. Rev. B **84**, 014521 (2011).
[16] X.-W. Yan, M. Gao, Z.-Y. Lu, and T. Xiang, Phys. Rev. B **83**, 233205 (2011).
[17] C. Cao and J. Dai, Phys. Rev. Lett. **107**, 056401 (2011).
[18] W. Li, S. Dong, C. Fang, and J. P. Hu, Phys. Rev. B **85**, 100407(R) (2012).
[19] D. Y. Liu, Y. M. Quan, Z. Zeng, and L. J. Zou, Physica B **407**, 1139 (2012).

[20]S. Maiti, M. M. Korshunov, T. A. Maier, P. J. Hirschfeld, and A. V. Chubukov, Phys. Rev. Lett. **107**, 147002 (2011).
[21]T. A. Maier, S. Graser, P. J. Hirschfeld, and D. J. Scalapino, Phys. Rev. B **83**, 100515(R) (2011).
[22]Y. Zhou, D. H. Xu, F. C. Zhang, and W. Q. Chen, Europhys. Lett. **95**, 17003 (2011).
[23]S. M. Huang and C. Y. Mou, Phys. Rev. B **84**, 184521 (2011).
[24]S. M. Huang and C. Y. Mou, Phys. Rev. B **85**, 184519 (2012).
[25]H. M. Jiang, W. Q. Chen, Z. J. Yao, and F. C. Zhang, Phys. Rev. B **85**, 104506 (2012).
[26]Neutron scattering data can be found in, for example, M. Wang, C. Fang, D.-X. Yao, G. T. Tan, L. W. Harriger, Y. Song, T. Netherton, C. Zhang, M. Wang, M. B. Stone, W. Tian, J. P. Hu, and P. Dai, Nat. Commun. **2**, 580 (2011); J. Zhao, D. T. Adroja, D.-X. Yao, R. Bewley, S. Li, X. F. Wang, G. Wu, X. H. Chen, J. P. Hu, and P. Dai, Nat. Phys. **5**, 555 (2009); J. Zhao, D.-X. Yao, S. Li, T. Hong, Y. Chen, S. Chang, W. Ratcliff, II, J. W. Lynn, H. A. Mook, G. F. Chen, J. L. Luo, N. L. Wang, E. W. Carlson, J. Hu, and P. Dai, Phys. Rev. Lett. **101**, 167203 (2008).
[27]K. Seo, B. A. Bernevig, and J. P. Hu, Phys. Rev. Lett. **101**, 206404 (2008).
[28]E. Berg, D. Orgad, and S. A. Kivelson, Phys. Rev. B **78**, 094509 (2008).
[29]Z. H. Liu, P. Richard, N. Xu, G. Xu, Y. Li, X. C. Fang, L. L. Jia, G. F. Chen, D. M. Wang, J. B. He, T. Qian, J. P. Hu, H. Ding, and S. C. Wang, Phys. Rev. Lett. **109**, 037003 (2012).
[30]Q. Wang, Z. Li, W. H. Zhang, Z. C. Zhang, J. S. Zhang, W. Li, H. Ding, Y. B. Ou, P. Deng, K. Chang, J. Wen, C. L. Song, K. He, J. F. Jia, S. H. Ji, Y. Y. Wang, L. L. Wang, X. Chen, X. C. Ma, and Q. K. Xue, Chin. Phys. Lett. **29**, 037402 (2012).